Combining extended x-ray absorption fine structure with numerical simulations for disordered systems

2005 J. Phys.: Condens. Matter 17 S145

(http://iopscience.iop.org/0953-8984/17/5/015)

INSTITUTE OF PHYSICS PUBLISHING JOURNAL OF PHYSICS: CONDENSED MATTER

J. Phys.: Condens. Matter **17** (2005) S145–S157 doi:10.1088/0953-8984/17/5/015

Combining extended x-ray absorption fine structure with numerical simulations for disordered systems

Guillaume Ferlat[1,4], **Jean-Christophe Soetens**[2], **Alfonso San Miguel**[3] and **Philippe Anthony Bopp**[2]

[1] Laboratoire de Minéralogie et Cristallographie de Paris, UMR Universités Paris 6 et 7—CNRS—IPGP no 7590, case 115, 4 place Jussieu, 75252 Paris cedex 05, France
[2] Laboratoire de Physico-Chimie Moléculaire, UMR Université Bordeaux I—CNRS no 5803, F-33405 Talence, France
[3] Laboratoire de Physique de la Matière Condensée et Nanostructures, UMR Université Claude Bernard Lyon I—CNRS no 5586, F-69622 Villeurbanne, France

E-mail: ferlat@lmcp.jussieu.fr

Received 3 November 2004, in final form 3 November 2004
Published 21 January 2005
Online at stacks.iop.org/JPhysCM/17/S145

Abstract

Over the past two decades x-ray absorption spectroscopy has proven to be a valuable tool for the study of the short-range order in a wide variety of materials, including disordered systems such as superionic conductors as well as glasses, amorphous and liquid systems in general. A number of methods have been proposed to analyse EXAFS data. However, in the case of disordered systems, only the ones taking the distribution of atomic environments into account should be retained. Molecular dynamics (MD) simulations are a valuable tool in this respect, as will be shown from results obtained in a supercritical aqueous solution.

1. Introduction

X-ray absorption spectroscopy (XAS) is a powerful structural technique for the investigation of the short-range environment around selected atomic species in condensed matter. This method's chemical selectivity is of particular interest since it allows one to deal with complex systems (containing a large number of elements) and with diluted samples. For such systems it appears very often that XAS is the only structural tool that can be easily used.

As a result of the x-ray induced excitation, a core electron is ejected from the absorber and is scattered by the potentials of the surrounding atoms. The quantum interference resulting from the photoelectronic wave scattering, visible in the XAS spectra and called EXAFS (extended x-ray absorption fine structure), is thus a probe of the absorber's local environment.

[4] Author to whom any correspondence should be addressed.

Complications in the data analysis arising when disordered environments are considered have been commented upon in the literature a great deal [1–4]. By *disordered environment* we mean here any system for which the distribution of neighbour-distances is continuous, i.e. where separate coordination shells cannot be distinguished. The overlap between coordination shells, (i.e. the deviation from zero of the radial pair distribution function's first minima), can be used as a measure of the extent to which the problem that we are considering is severe.

In spite of the direct relationship between the EXAFS signal and the distributions of neighbours around the absorber (see equations (4) and (6) in the next section), it is generally not possible for these systems to carry out a straightforward Fourier transformation of the experimental signal. This inversion belongs to the class of *ill-defined* problems [5]: the limited data range, and in particular the loss of low k information (this energy region being dominated by multiple scatterings), does not allow for a unique determination of the real space solutions. This imposes the use of constrained methods to analyse the data. For instance, regularization methods, which are non-parametric and which allow the imposition of physical constraints in a systematic way, were proposed more than two decades ago [5, 6]. In the same spirit, wavelet transform methods [7, 8] were recently proposed as alternatives to Fourier transforms within the EXAFS analysis context. However, both regularization [9–12] and wavelet methods [13–15] have scarcely been used so far, and more work is needed.

Ideally, the required methods of analysis should be able to deal with the lack of long/middle-range information in the EXAFS data and to provide a sensible description of the continuous distribution of environments in such systems. Due to the errors associated with the Fourier transformation of a data set of limited k-range, *inverse* methods, i.e. methods starting from a real-space model and carrying the data over into k-space, should be encouraged. As will be seen in the next section, the structure functions dampen out rather quickly in r-space for such systems. Furthermore, it is straightforward to extend the r-range if necessary, and numerical simulations such as molecular dynamics (MD) or Monte Carlo (MC) are in this respect useful tools. They were used as early as 1980 [16] to support EXAFS analysis. However, intimate combinations of MD/MC-EXAFS such as the one used in section 3 have become feasible only in the last decade, due to both the increasing advance of computational capabilities and the development of modern XAS algorithms allowing one to exploit as much as possible the symbiosis.

In this paper, we shall first briefly review the methods used to combine EXAFS with numerical calculations. We then concentrate on some results obtained from our investigations of supercritical aqueous electrolytes [17–20]. The combined use of molecular dynamics calculations and EXAFS experiments appears to be not only a powerful tool but also a didactic means to illustrate the strengths and limitations of the x-ray absorption spectroscopy for the study of highly disordered materials. Finally, we conclude with some remarks about alternate methodologies, which may develop in the future.

2. Combining numerical simulations with EXAFS

Numerical simulations such as molecular dynamics (MD) or Monte Carlo (MC) calculations [21] allow one to sample the phase space accessible to the system of interest under given thermodynamic conditions. The required input data comprise an initial configuration constructed from a box containing a given number of atoms and, for classical simulations, a set of interatomic potentials. *Ab initio* MD simulations [22–24] solve the Schrödinger equation for the system of electrons contained in the box and thus do not use interatomic potentials; however, usually only the valence electrons are considered, which leads to the introduction of pseudo-potentials to replace the screened core electrons.

In MC simulations, the atoms are randomly moved and the displacements accepted with statistical weights fixed by the ensemble one wants to sample (e.g. the canonical NVT ensemble). In classical MD simulations, the forces acting on the atoms are calculated at equally spaced intervals of time, and the atoms moved according to Newton's equation. In *ab initio* simulations, the forces acting on the ions are calculated by using the Hellmann–Feynman theorem.

In all cases an ensemble of microscopic configurations is retrieved from which one can compute any structural ensemble-averaged observable, e.g. the EXAFS signal.

This allows for the determination of *synthetic* EXAFS spectra in which the effects of the disorder (i.e. the heterogeneity of the environments) are intrinsically taken into account. Thus, the comparison of computed and experimental spectra constitutes a much more robust way to analyse data than the unconstrained peak fitting approaches. Conversely, the experimental information can be used to check the reliability of the intermolecular potentials used in the simulations [25–27].

In the recent years, the number of studies combining MD [17–19, 25, 26, 28–66] (and, to a much lesser extent, MC [67–69]) simulations with EXAFS has considerably increased due to the advance of modern XAS algorithms. Two methodologies have been employed which use either a set of clusters extracted from the sampled configurations or the averaged structure description in terms of radial pair distribution functions $g(r)$.

2.1. Analysis from a set of clusters

Clusters centered at the x-ray absorbing atoms (denoted α) can be extracted from the configurations generated in a simulation. Each cluster defines a set of neighbouring atoms located at positions $\mathbf{r_j}$ relative to the photoelectron source at $\mathbf{r_0}$. For each cluster, an individual EXAFS spectrum, $\chi_c(k)$, can be generated; it results from the contributions from all the possible scattering paths starting and ending at the absorber site:

$$\chi_c(k) = \sum \chi_2(k) + \sum \chi_3(k) + \sum \chi_4(k) + \mathrm{O}(\chi_5), \tag{1}$$

where $k = \sqrt{2m(E - E_0)}/\hbar$ is the modulus of the photoelectron wavevector (E_0 is the threshold energy). In equation (1), the subscript stands for the number of *legs* involved in the scattering path: the first term is the contribution from single scatterings (two legs), the second from three-legged multiple scatterings, etc.

Restricting the summation to single scattering (SS) contributions, the individual EXAFS spectrum for each cluster can be written as

$$\chi_c(k) = \sum_j^{\text{paths}} S_0^2(k) \frac{1}{kR_j^2} \exp(-2R_j/\lambda(R_j, k)) |f_j^{\text{eff}}(k, R_j)| \sin(2kR_j + \phi_j(k, R_j)), \tag{2}$$

where j goes over the paths; R_j is half its total length ($R_j = |\mathbf{r_j} - \mathbf{r_0}|$ in the case of SS paths), and $|f_j^{\text{eff}}|$ and ϕ_j are the effective scattering amplitude and net phase functions, respectively, of path j.

It has been shown [70] that each multiple scattering (MS) gives rise to an oscillating contribution, which can be expressed in a form analogous to that of the single scattering. Thus, provided that the MS expansion converges (a condition which is usually fulfilled in the medium/high energy range of the spectrum, typically for $k > 3$ Å), the above expression can be extended to MS contributions as well [3, 70] (using the scattering matrix algorithm of Rehr and Albers [71, 72]).

The average over all the individual spectra,

$$\langle \chi_\alpha(k) \rangle = \frac{1}{N_{\text{cluster}}} \sum_{c}^{N_{\text{cluster}}} \chi_{\text{c}}(k), \tag{3}$$

provides an EXAFS spectrum which can be compared to the experimental one.

In this method, the disorder is taken into account by summing over a number of structural arrangements. Provided the sampling is representative, there is no need for further adjustments, e.g. through Debye–Waller factors in equation (2).

This method was pioneered by Palmer *et al* [54] and subsequently used by different groups [17, 18, 26, 55–58, 60–66, 68, 69, 73]. Most of these works were devoted to the elucidation of the hydration structure around ions in aqueous solutions. The possibility to detect very fine effects such as the contribution from the second water shell was addressed, and multiple-scattering contributions from the first shell have been investigated as well as the contributions from the water hydrogens.

All authors used the FEFF code [71, 74], which allows for the calculation of the effective scattering amplitude $|f_{\text{eff}}(k, R_j)|$ and phase $\phi_j(k, R_j)$ associated to each path in equation (2) and an efficient selection of the main scattering paths. The calculations of the scattering potentials can be carried out using a full *ab initio* self-consistent field (SCF) scheme or using the common *muffin-tin* (MT) approximation (overlapping of spherically averaged atomic potentials).

Several practical questions must be addressed, such as the determination of the sampling interval and the total sampling length. In practice it is found that snapshots taken every 0.2 ps from an MD simulation run yield to a more or less statistically independent set of configurations. Yet the total number of spectra required can be huge in labile structures such as the ones encountered in aqueous solutions (typically, a minimum of 500–1000 spectra should be used [17, 64]). Of course, these figures are dependent upon the amount of fluctuations in the absorber's environment (in other words, upon the strength of the interactions within the first coordination shell).

Due to the local character of the EXAFS technique, the clusters' minimal size can be small (distances of the order of 5 Å for disordered systems). However, when using the MT approximation, artefacts due to a too short truncation can occur: this is due to the fact that for an accurate determination of the MT radii the full environment of the scatterers is needed. This means that the full second coordination shell, at least, should be included in the clusters, even if the scattering contributions come solely from the first neighbours. Such effects were visible for cluster radii smaller than 8 Å in the case of the bromide solvation [20].

Since it is possible to include n-legged paths up to any desired order, this methodology is convenient for exploring the contributions from multiple scatterings. It is also well adapted to investigating the effects of different local environments (due to static or dynamic fluctuations) [17, 68]. It is furthermore possible to calculate the partial contributions from the different types of scatterers by selecting the appropriate paths. However, it should be noted that in this case all species should still be included at the level of the potentials since a straightforward removing of the undesired atoms would distort the charge density calculations by creating artificial holes.

The main drawback of this method is its computational cost. Computing thousands of spectra may appear intractable in some cases, especially when using SCF calculations and/or including high-order MS contributions. Tricks such as computing the potentials from one representative cluster and using them for all clusters can be used, but the relevancy of these approximations should be checked in the case of highly disordered systems.

2.2. Analysis from a set of g_n functions

The average atomic structure seen from a given atom can be described using *many-body* distribution functions, hereafter called g_n. These functions can be easily calculated from the atomic coordinates saved during a simulation. For instance, the $g_2(r)$ function, usually called the radial pair distribution function (RDF), is a normalized histogram of interatomic distances. Similarly, $g_3(r_1, r_2, \theta)$ is a triplet distribution (or a 3D normalized histogram of interatomic angles).

The g_n distributions allow one to calculate any structurally averaged quantity. In particular, the EXAFS signal is given, for a monatomic system by [4, 75]

$$\langle \chi(k) \rangle = \int \mathrm{d}r\, 4\pi\rho r^2 g_2(r)\gamma^{(2)}(k, r) + \int \mathrm{d}r_1\, \mathrm{d}r_2\, \mathrm{d}\theta\, 8\pi^2 r_1^2 r_2^2 \sin(\theta)\rho^2 g_3(r_1, r_2, \theta)\gamma^{(3)}(r_1, r_2, \theta, k) + \cdots, \tag{4}$$

where ρ is the number density and the $\gamma^{(n)}$ functions are oscillating functions which represent the irreducible n-body contributions [75] to the EXAFS signal (contributions from n higher than 3 have been omitted). Thus, the first term in equation (4) stands for all possible scattering contributions (SS and MS) involving the absorber and one scatterer, the second term represents MS contributions involving the absorber and two scatterers, etc. The first term is most often the leading term and the higher order terms are then not considered in the EXAFS analysis. However, these terms are not always negligible (for instance when dealing with liquid metals or with the well defined hydration structures of transition-metal ions) and the sensitivity of EXAFS to such contributions has sometimes been exploited to retrieve triplet correlations (see e.g. [33, 76–78]).

Restricting the discussion now to two-body terms, we shall consider the case of an N-component system. The average atomic structure seen from any α-particle is described by the set of $\frac{N(N-1)}{2}$ partial radial distribution functions (PRDFs) $g_{\alpha\beta}(r)$, where β runs over all the species in the system. The $g_{\alpha\beta}(r)$ PRDF is obtained from the simulated coordinates by counting the number of β particles located at distances between r and $r+\mathrm{d}r$ from any α particle and by normalizing this number by the corresponding value for a uniform gas of density ρ_β:

$$g_{\alpha\beta}(r) = \frac{\mathrm{d}N_\beta(r, r+\mathrm{d}r)}{4\pi\rho_\beta r^2\, \mathrm{d}r}. \tag{5}$$

The EXAFS partial contribution $\langle \chi_{\alpha\beta}(k) \rangle$ from each scatterer β around the x-ray absorber species α is thus given by [19, 79]

$$\langle \chi_{\alpha\beta}(k) \rangle = \int_0^{r_{\alpha\beta}} 4\pi\rho_\beta r^2 g_{\alpha\beta}(r)\gamma^{(2)}_{\alpha\beta}(k, r)\, \mathrm{d}r, \tag{6}$$

where $\gamma^{(2)}_{\alpha\beta}(k, r)$ is the EXAFS signal corresponding to a single atom pair at distance r. The total EXAFS spectrum, $\langle \chi_\alpha(k) \rangle$, calculated at a given absorption edge (e.g. K-edge) of the α species is then obtained from the summation over all the scatterers:

$$\langle \chi_\alpha(k) \rangle = \sum_\beta \langle \chi_{\alpha\beta}(k) \rangle. \tag{7}$$

The kernel of the integral in equation (6) can be written [75]

$$\gamma^{(2)}_{\alpha\beta}(k, r) = A_{\alpha\beta}(k, r)\sin(2kr + \phi_{\alpha\beta}(k, r)), \tag{8}$$

where $A_{\alpha\beta}(k, r)$ and $\phi_{\alpha\beta}(k, r)$ are the EXAFS amplitude and phase functions of an α–β cluster, respectively. ($A_{\alpha\beta}(k, r)$ is related to $S_0^2(k)\frac{1}{kR^2}\exp(-2R/\lambda(R, k))|f_{\mathrm{eff}}(k, R)|$ in equation (2).)

Due to the short-range character of this kernel, the upper limit of integration $r_{\alpha\beta}$ corresponds typically, in liquid systems, to the first minimum of $g_{\alpha\beta}(r)$. In highly disordered systems, values even smaller than the ones assumed in the next section can be used. However, from a practical point of view, a large value of $r_{\alpha\beta}$ should be used (typically 10 Å) to ensure that the calculation converges. Furthermore, the $g(r)$ integration cannot be sharply truncated, and thus a Gaussian semi-window is used at high r to avoid termination ripples [80].

The relation between the EXAFS signal and the partial radial distribution functions was available in the early 1980s [81, 82]. The use of theoretical $g(r)$ obtained from physically sound models [83, 84] or from MD simulations [16] to support the EXAFS analysis can be traced back to that period. However, a major advance towards the consistent use of these approaches has been achieved in the last decade [79] with the advance of the GNXAS set of programs [75, 80, 85], which explicitly makes use of the g_n functions to perform accurate MS EXAFS calculations of the XAS cross-section.

Combinations of MD or MC simulations with GNXAS have been applied to a large range of disordered systems (e.g. [19, 28–40, 42–48, 51, 53, 67]). This methodology has several advantages over the one described above. First, the calculation of the average EXAFS signal is straightforward and time inexpensive (as soon as the g_n functions have been obtained). Moreover, the configurational average of the MS contributions is treated on a more rigorous basis. Second, it allows very easily for the identification of the partial $\langle\chi_{\alpha\beta}(k)\rangle$ contributions of interest.

2.3. Refining the simulated model

The comparison of the calculated and experimental EXAFS signals provides a stringent test of the 'low-r part' of the simulated model and thus mostly of the short-range part of the interatomic potentials. This information can be used when the simulations are wide of the mark to refine the potentials until a satisfactory agreement is reached. However, such iterative procedures might be very time expensive. More simply, the experimental information can be used to refine the simulated outputs (atomic coordinates or RDFs).

One could think of using the simulated atomic coordinates as a starting input for a reverse Monte Carlo (RMC) analysis of the EXAFS data [86]. Such a coupling of MD and RMC has been used for the analysis of x-ray diffraction data of glasses [87]; this allowed the identification of the pair potentials requiring optimization, and a potential fitting step was then introduced in the methodology [88]. However, we do not know of any work having used an MD-RMC combination for EXAFS data.

One simple approach is to shift and/or modify the shape of the RDF's first peak so as to reach an agreement with the EXAFS experiment [19]. Within the GNXAS framework, an iterative and automated method allowing for the refinement of the simulated $g(r)$ was proposed ten years ago [28]. The initial model $g(r)$ is split into a short-range part to be refined (typically the first peak of $g(r)$) and a remaining contribution (*tail*). The short-range part is modelled by several (usually one or two) short-range peaks, using Γ-like functions [28, 76]. The EXAFS signals associated with each contribution (short-range peaks and tail) are then calculated and the parameters describing the peaks are varied in an iterative process to improve the agreement with the experimental $\langle\chi(k)\rangle$ while keeping the tail contribution fixed. In this way, the refinement of the short-range part (to which EXAFS is very sensitive) is anchored to the middle/long-range part (to which EXAFS is almost blind) provided by the initial model. The reconstructed distribution obviously fulfils the constraint $\lim_{r\to\infty} g(r) = 1$.

A variation of this method has been proposed, initially for mono-component systems [79], which allows one to further constrain the shape of the reconstructed distribution by forcing it to

satisfy thermodynamic limits: constraints on the coordination numbers and higher even-order moments of the reconstructed distribution are derived from the compressibility rule (given by the low q limit of the structure factor, $\langle S(q)\rangle$. Here q stands for the scattering wavevector modulus). This methodology was later extended to ionic binary salts [89] and very recently to any binary mixture [90] (the constraints on the structural parameters are obtained in this latter case from the long wavelength limits of the Bathia–Thornton structure factors [91]). As pointed out by these authors, the reduction in the number of free parameters and thus in the uncertainty in the shape of the reconstructed distribution is an important point, especially for liquids. In the case of multicomponent systems, it is also possible to take into account the constraint $g_{AB}(r) = g_{BA}(r)$ by adjusting simultaneously a set of data acquired at one (or more) absorption edge of each element A and B (multiple-edge analysis [89, 92]).

The initial $g(r)$ for this analysis can be obtained from diffraction data, simulations or any other type of calculations. Clearly, the reliability of the final $g(r)$ in the long-distance range will be strongly dependent on this original model. Thus, numerical simulations are particularly helpful when diffraction experiments cannot be handled (e.g. in low concentrated solutions or in complex systems).

3. A case study: supercritical aqueous solutions

We shall now focus on the hydration structure of the bromine ion at high temperature and low density. We shall show that this structure cannot be defined unambiguously by EXAFS alone; the use of the MD-EXAFS combination appears mandatory to constrain the analysis since there is no other experimental information available for this system in these conditions.

3.1. Methods

EXAFS experiments at the Br K-edge in a diluted (0.2 molal) RbBr–H_2O solution were carried out in ambient ($\rho \sim 1$ g cm^{-3}) and supercritical ($\rho \sim 0.4$ g cm^{-3}) conditions at the ESRF beamline BM32. We shall concentrate on the latter conditions, which correspond to $T = 450\,^{\circ}$C and $p = 450$ bar. In these conditions, the usable data range obtained in a former investigation [17] was limited to about $k_{min} = 2.5$ and $k_{max} = 6$ Å^{-1}; in a subsequent investigation [19] the higher quality of the data enabled us to extend k_{max} up to 10 Å^{-1}.

Classical MD simulations were performed at the corresponding thermodynamic conditions ($T = 450\,^{\circ}$C, $\rho \sim 0.4$ g cm^{-3}) for 800 ps on a system containing 452 water molecules and two Rb^+Br^- ion pairs. The parameters used for the interatomic potentials are described in [17]. Atomic configurations were saved every 0.2 ps. MD-EXAFS spectra have been calculated using both methods (clusters and $g(r)$) described above. For the first method, 8000 clusters were extracted from the trajectory and used as input for the FEFF code [74]. An excellent agreement was obtained between SCF and MT calculations [20]. In the latter case, it was found that a radius of at least 8 Å was necessary to avoid artefacts in the calculations (resulting in slight distortions of the smoothness of the dominating oscillation). An SCF radius of 4.5 Å was used in the former case. Hydrogen scattering contributions were removed in the MT calculations. Contributions from oxygen MS scattering were found to be negligible. For the second method, all $g_{Br-\beta}(r)$ PRDFs (β = O, H, Br, Rb) were injected into equation (6). The total average signal obtained (equation (7)) is in good agreement[5] with the one obtained from the clusters' average [20], thereby demonstrating the equivalency of both methodologies.

[5] Except at low k values where a slight mismatch of the leading frequency was observed, due to, most likely, the slightly different strategies in both methods to compute the muffin-tin parameters.

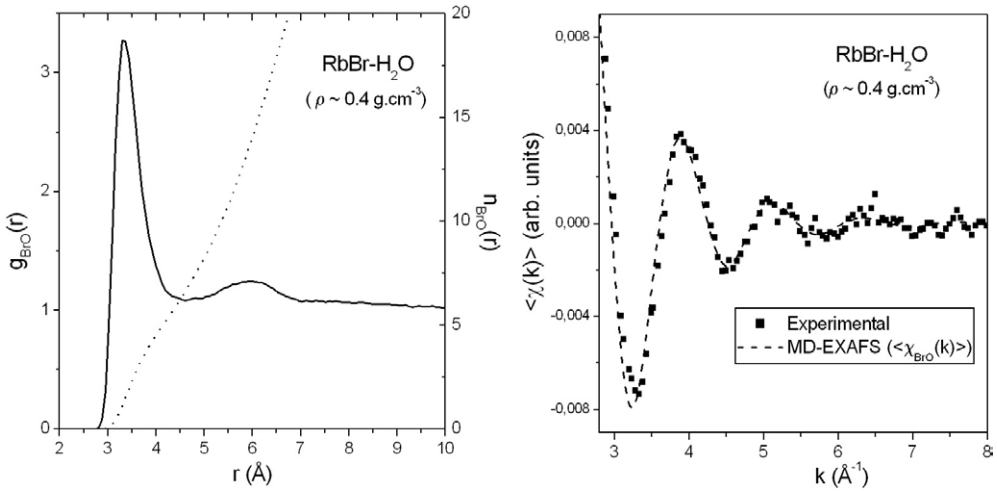

Figure 1. Left-hand panel: partial radial distribution function $g_{\mathrm{BrO}}(r)$ obtained from the MD simulations in the RbBr–H_2O solution (0.2 molal) in supercritical conditions. The running coordination number, $n_{\mathrm{BrO}}(r)$, is shown with dots (right-hand scale). It is defined by equation (9). Right-hand panel: comparison of the EXAFS experimental (■) and simulated $\langle\chi_{\mathrm{BrO}}(k)\rangle$ spectra.

From the EXAFS point of view, the main contribution in the experimental signals arises from the water oxygens. (The scattering power from the water hydrogens is too weak and the ion–ion contributions are almost negligible at this concentration. However, see [19] for a more detailed discussion of these contributions.) Thus, the experimental EXAFS signal can be reproduced within experimental accuracy by integrating solely the Br–O PRDF (equation (6)), see figure 1, right-hand panel. The running coordination number, $n_{\mathrm{BrO}}(r)$, referred to in the left-hand panel, is defined by

$$n_{\mathrm{BrO}}(r) = 4\pi\rho_{\mathrm{O}} \int_0^r g_{\mathrm{BrO}}(r')r'^2\,\mathrm{d}r', \tag{9}$$

where ρ_{O} is the number density of water oxygen.

3.2. Discussion

The $g_{\mathrm{BrO}}(r)$ obtained in supercritical conditions is shown in figure 1, left-hand panel. Note that the first peak is very broad and cannot be clearly resolved from the second one since the first minimum is not well defined (it is located somewhere between 4.4 and 4.9 Å). This reflects the high mobility of the water molecules in the neighbourhood of the ion. As a result, any geometrically defined coordination number for the first shell is poorly defined: it varies from 5 to 8 depending on the upper limit of integration of the $g(r)$. We have studied the distributions of the relative positions of the first seven oxygen neighbours: the first neighbours of each Br^- are determined, their distances are ordered and binned individually for each neighbour. The distributions thus obtained, hereafter denoted $g^i_{\mathrm{BrO}}(r)$, are shown in figure 2, left-hand panel, together with the total $g_{\mathrm{BrO}}(r)$ PRDF. They overlap because of both spatial[6] and time[7] fluctuations of the oxygen positions within the first coordination shell. One can note that

[6] For instance, it may happen that the first neighbour of a particular Br^- is found at a larger distance than the second neighbour of another Br^-.

[7] For instance, it may happen that the first neighbour of a particular Br^- is, at a later time, at a larger distance than was the second neighbour at the former time.

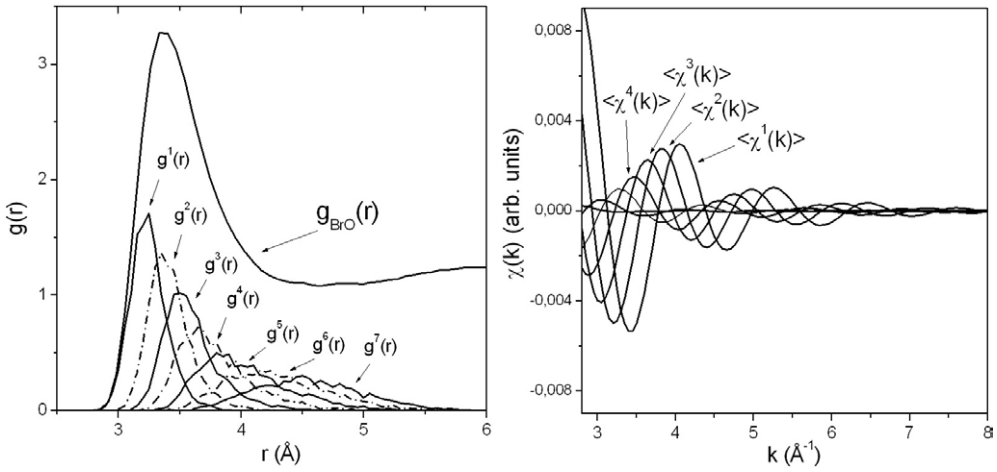

Figure 2. Left-hand panel: distributions of the positions of the seven first oxygen neighbours, $g^i_{\mathrm{BrO}}(r)$, within the first Br–O coordination shell, obtained from the MD simulations. Right-hand panel: corresponding EXAFS partial contributions $\langle\chi^i_{\mathrm{BrO}}(k)\rangle$ (obtained from the integration of $g^i_{\mathrm{BrO}}(r)$, equation (6)). Note that these contributions are marginal for $i > 5$.

these distributions are quite broad, especially for the more distant neighbours ($i = 5, 6, 7$), illustrating the fluctuations in the bromine local environment. Similar decompositions of a $g_{\alpha\beta}(r)$ PRDF into its $g^i_{\alpha\beta}(r)$ contributions can be found in other works (e.g. for water [93], Se [68], Te [94], GeSe [95]).

Since the first peak of $g_{\mathrm{BrO}}(r)$ extends beyond 4 Å one may question the possibility of resolving the entire distribution of neighbours by EXAFS. Indeed, the higher r part of the $g(r)$ considered here is likely to give a very small contribution to the $\langle\chi(k)\rangle$ EXAFS signal. Valuable insight into this problem can be obtained from the decomposition of the $g_{\mathrm{BrO}}(r)$ function into its $g^i_{\mathrm{BrO}}(r)$ contributions. Inserting each $g^i_{\mathrm{BrO}}(r)$ into equation (6), all partial contributions $\langle\chi^i_{\mathrm{BrO}}(k)\rangle$ to the total EXAFS $\langle\chi_{\mathrm{BrO}}(k)\rangle$ spectrum have been calculated. The resulting signals are shown in figure 2, right-hand panel. Not surprisingly, the $\langle\chi^i_{\mathrm{BrO}}(k)\rangle$ signals are quickly smeared out as i increases (from 1 to 7). The main contributions come from the three first neighbours.

Figure 3, left-hand panel, shows the distributions $g^{1-j}_{\mathrm{BrO}}(r)$ obtained by summing up the first j partial contributions ($\sum_{i=1}^{j} g^i_{\mathrm{BrO}}(r)$). These distributions have been used in equation (6) to obtain the signals $\langle\chi^{1-j}_{\mathrm{BrO}}(k)\rangle$ shown in figure 3, right-hand panel. Equivalently, these signals could have been obtained from the summation of the j first partial contributions ($\sum_{i=1,j}\langle\chi^i_{\mathrm{BrO}}(k)\rangle$). One notes that the quantity $\langle\chi^{1-j}_{\mathrm{BrO}}(k)\rangle$ quickly converges (to the total $\langle\chi_{\mathrm{BrO}}(k)\rangle$ signal) as j increases: $\langle\chi^{1-6}_{\mathrm{BrO}}(k)\rangle$ is not distinguishable from $\langle\chi^{1-5}_{\mathrm{BrO}}(k)\rangle$; $\langle\chi^{1-3}_{\mathrm{BrO}}(k)\rangle$ differs only by a small variation in amplitude. This means that the main features (position and amplitude of the oscillations) of the total EXAFS signal are reasonably well reproduced as soon as the distribution of the first three neighbours are taken into account. This distribution, however, represents only a fraction of the full first coordination shell. This confirms that the EXAFS signal is highly sensitive to the rise and amplitude of the first peak of $g(r)$ but almost blind to the details of its shape beyond the first maximum. Similar findings were obtained in other disordered systems, for instance in liquid germanium [4] or in silicate glasses [52].

This shows the limitation to our ability to resolve such a coordination shell by the use of EXAFS alone. Suppose that the $g_{\mathrm{BrO}}(r)$ shown in figure 1 is the *true* distribution and thus that

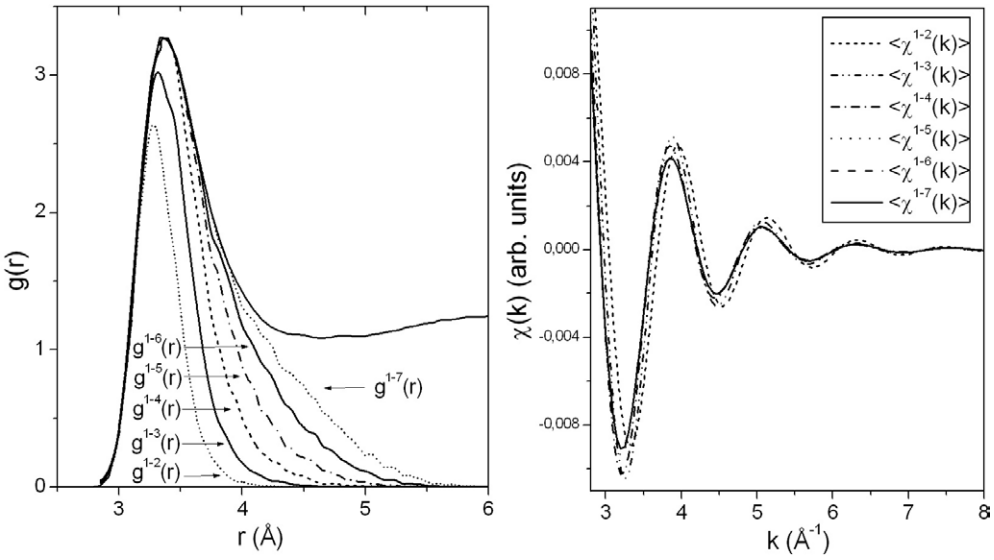

Figure 3. Left-hand panel: distributions of all positions from the first to the jth oxygen neighbours, $g_{\mathrm{BrO}}^{1-j}(r)$, obtained from the MD simulations. Right-hand panel: corresponding EXAFS contributions $\langle\chi_{\mathrm{BrO}}^{1-j}(k)\rangle$ (obtained from the integration of $g_{\mathrm{BrO}}^{1-j}(r)$, equation (6)). Note that these contributions converge as soon as $j > 4$.

the MD $\langle\chi_{\mathrm{BrO}}(k)\rangle$ is the *perfect* experimental signal one could hope to get from a measurement with zero noise. Inverting equation (6) to retrieve the RDF is fundamentally unstable since the result can be anything between $g_{\mathrm{BrO}}^{1-5}(r)$ and $g_{\mathrm{BrO}}^{1-8}(r)$. In practice, there will always be some noise (and possibly some errors) affecting the experimental data which will further increase the variability of the solutions. For instance, $g_{\mathrm{BrO}}^{1-3}(r)$ can reproduce the experimental data shown in figure 1 (right-hand panel) within the experimental error bars (given the uncertainty associated with the extraction of the experimental signal). Given the much lower signal to noise ratio of earlier experiments [17, 55], it is not surprising that a very low (and unrealistic) coordination number ($\sim$2) was obtained from a standard EXAFS analysis (cumulant expansion) [55].

Note also that the asymmetry of a given distribution is not always reflected in the EXAFS data: symmetric distributions, such as $g_{\mathrm{BrO}}^{1-3}(r)$, can reproduce the experimental data although the actual distribution may also be the highly asymmetric $g_{\mathrm{BrO}}^{1-8}(r)$. This invalidates a quite common argument in the literature, namely that when the asymmetry parameter (the third cumulant within a cumulant analysis) is found to be negligible or not necessary for the data fitting, the distribution of neighbours is Gaussian: this argument is unfortunately not conclusive.

This urges the use of careful methods of analysis when dealing with disordered systems. From the information contained in the EXAFS data, one can get very accurate information on the *low-r side* of $g(r)$ (say the shape of the distribution up to, typically, the first maximum). The EXAFS data are generally not suitable for retrieving the *high-r side* of $g(r)$ (typically, beyond the first maximum). This implies that attempts to fit the EXAFS data by isolated peaks models (on a $g(r) = 0$ baseline) are irrelevant for these systems, whatever the functional form used to model the peaks. Such unsuitable models almost always tend to provide narrower distributions than the actual ones (resulting in underestimated coordination numbers and mean interatomic distances). In any case, as pointed out elsewhere [4], one needs to take into account

the continuous distribution of distances which characterize the structure of disordered systems. These considerations are at the heart of the methodology proposed in [28, 79]: an external model $g(r)$ is used as a starting distribution in a refinement process which allows the low-r part of this model to be varied on top of a realistic baseline (provided by the model middle/long-range part, which is kept fixed). In this way, a continuous distribution is constructed.

The present considerations, although derived from an extreme case study (high temperature liquid with weak average intermolecular interactions) and chosen here for didactic purposes, are of general relevance. They apply to a large class of so-called *ill-ordered* systems.

4. Conclusions

The strengths and limitations of x-ray absorption spectroscopy are now well understood [3, 4] and an increasing number of studies combining XAS with other experimental or numerical techniques have appeared in the last ten years. Despite being very promising, the RMC method has so far not been much used for EXAFS analysis [15, 86, 96–100]. It is clear that for disordered systems special care has to be taken since the information contained in the EXAFS data will most often not be sufficient to constrain the RMC fit. However, the simultaneous RMC analysis of EXAFS and diffraction data [96, 99, 100] appears to be a very attractive tool and a good alternative to peak-fitting methods. Numerical simulations are a natural complement to RMC and could be used in conjunction: similarly to what has been done for the analysis of diffraction data $\langle S(q)\rangle$ [87], one could think of using the RMC method to refine a starting configuration obtained from MD (or MC) simulations for the analysis of EXAFS $\langle \chi(k)\rangle$. This could then be exploited in a refinement process of the interatomic potentials used in the simulations [88]. There is no doubt that these and similar methods will play a growing role in the next few years.

Acknowledgments

GF is grateful to Daniel Bowron and Simone de Panfilis for the help provided in the use of the GNXAS set of codes. We also acknowledge the authors of [90] for providing their manuscript prior to publication.

References

[1] Crozier E D, Rehr J J and Ingalls R 1988 *X-ray absorption: Principles, Applications, Techniques of EXAFS, SEXAFS and XANES* ed D Koningsberger and R Prins (New York: Wiley) chapter 9
[2] Crozier E D 1995 *Physica* B **208/209** 330
[3] Crozier E D 1997 *Nucl. Instrum. Methods* B **133** 134
[4] Filipponi A 2001 *J. Phys.: Condens. Matter* **13** R23
[5] Babanov Y A, Vasin V V, Ageev A L and Ershov N V 1981 *Phys. Status Solidi* b **105** 747
[6] Ershov N V, Ageev A L, Vasin V V and Babanov Y A 1981 *Phys. Status Solidi* b **108** 103
[7] Shao X, Shao L and Zhao G 1998 *Anal. Commun.* **35** 135
[8] Yamaguchi K, Ito Y, Mukoyama T, Takahashi M and Emura S 1999 *J. Phys. B: At. Mol. Opt. Phys.* **32** 1393
[9] Ageev A, Babanov Y A, Vasin V V, Ershov N V and Serikov A 1983 *Phys. Status Solidi* b **117** 345
[10] Babanov Y A, Ershov N V, Schvetsov V R, Serikov A V, Ageev A L and Vasin V V 1986 *J. Non-Cryst. Solids* **79** 1
[11] Babanov Y A, Schvetsov V R and Sidorenko A F 1995 *Physica* B **208/209** 375
[12] Yang D S and Bunker G 1996 *Phys. Rev.* B. **54** 3169
[13] Muñoz M, Argoul P and Farges F 2003 *Am. Mineral.* **88** 694
[14] Muñoz M, Farges F and Argoul P 2004 *XAFS 12: Proc. 12th Int. Conf. on X-ray Absorption Fine Structure*; *Phys. Scr.* at press

[15] Berrodier I, Farges F, Benedetti M, Winterer M, Brown G E Jr and Deveughèle M 2004 *Geochim. Cosmochim. Acta* **68** 3019
[16] Hayes T M and Boyce J B 1980 *J. Phys. C: Solid State Phys.* **13** L731
[17] Ferlat G, San Miguel A, Jal J-F, Soetens J-C, Bopp P A, Daniel I, Guillot S, Hazemann J-L and Argoud R 2001 *Phys. Rev.* B **63** 134202
[18] Ferlat G, San Miguel A, Soetens J-C and Bopp P A 2002 *High Pressure Res.* **22** 399
[19] Ferlat G, San Miguel A, Jal J-F, Soetens J-C, Bopp P A, Hazemann J-L, Testemale D and Daniel I 2002 *J. Mol. Liq.* **101** 127
[20] Ferlat G 2002 *PhD Thesis* Université Claude Bernard Lyon I
[21] Frenkel D and Smit B 2001 *Understanding Molecular Simulations. From Algorithms to Applications* 2nd edn (London: Academic)
[22] Payne M C, Teter M P, Allan D C, Arias T A and Joannopoulos J D 1992 *Rev. Mod. Phys.* **64** 1045
[23] Tuckerman M E 2002 *J. Phys.: Condens. Matter* **14** R1297
[24] Tse J S 2002 *Annu. Rev. Phys. Chem.* **53** 249
[25] Roccatano D, Berendsen H J C and D'Angelo P 1998 *J. Chem. Phys.* **108** 9487
[26] Hoffmann M M, Darab J G, Palmer B J and Fulton J L 1999 *J. Phys. Chem.* A **103** 8471
[27] Laskowski R, Rybicki J, Chybicki M and Di Cicco A 2000 *Phys. Status Solidi* b **217** 737
[28] D'Angelo P, Di Nola A, Filipponi A, Pavel N V and Roccatano D 1994 *J. Chem. Phys.* **100** 985
[29] D'Angelo P, Di Nola A, Giglio E, Mangoni M and Pavel N 1995 *J. Phys. Chem.* **99** 5471
[30] D'Angelo P, Di Nola A, Mangoni M and Pavel N 1996 *J. Chem. Phys.* **104** 1779
[31] D'Angelo P, Nolting H-F and Pavel N 1996 *Phys. Rev.* A **53** 798
[32] D'Angelo P, Pavel N, Roccatano D and Nolting H-F 1996 *Phys. Rev.* B **54** 12129
[33] D'Angelo P and Pavel N 1999 *J. Chem. Phys.* **111** 5107
[34] D'Angelo P and Pavel N 1999 *J. Synchrotron Radiat.* **6** 281
[35] D'Angelo P and Pavel N 2001 *J. Synchrotron Radiat.* **8** 173 and references therein
[36] D'Angelo P, Barone V, Chillemi G, Sanna N, Meyer-Klaucke W and Pavel N 2002 *J. Am. Chem. Soc.* **124** 1958
[37] Chillemi G, D'Angelo P, Pavel N V, Sanna N and Barone V 2002 *J. Am. Chem. Soc.* **124** 1968
[38] Filipponi A and Di Cicco A 1995 *Phys. Rev.* B **51** 12322
[39] Di Cicco A 1996 *J. Phys.: Condens. Matter* **8** 9341
[40] Di Cicco A, Rosolen M J, Marassi R, Tossici R, Filipponi A and Rybicki J 1996 *J. Phys.: Condens. Matter* **8** 10779
[41] Di Cicco A and Minicucci M 1999 *J. Synchrotron Radiat.* **99** 255
[42] Di Cicco A, Aquilanti G, Minicucci M, Filipponi A and Rybicki J 1999 *J. Phys.: Condens. Matter* **11** L43
[43] Aquilanti G, Di Cicco A, Minicucci M, Filipponi A and Rybicki J 1999 *J. Synchrotron Radiat.* **6** 251
[44] Di Cicco A, Taglienti M, Minicucci M and Filipponi A 2000 *Phys. Rev.* B **62** 12001
[45] Rybicki J, Rybicka A, Witkowska A, Bergmański G, Di Cicco A, Minicucci M and Mancini G 2001 *J. Phys.: Condens. Matter* **13** 9781
[46] Trapananti A, Di Cicco A and Minicucci M 2002 *Phys. Rev.* B **66** 014202
[47] Di Cicco A, Minicucci M, Principi E, Witkowska A, Rybicki J and Laskowski R 2002 *J. Phys.: Condens. Matter* **14** 3365
[48] Kuzmin A, Obst S and Purans J 1997 *J. Phys.: Condens. Matter* **9** 10065
[49] Galoisy L, Delaye J M, Ghaleb D, Calas G, Le Grand M, Morin G, Ramos A and Pacaud F 1998 *Mater. Res. Soc. Symp. Proc.* **506** 133
[50] Rossano S, Ramos A, Delaye J-M, Filipponi A, Creux S, Brouder C and Calas G 1999 *J. Synchrotron Radiat.* **6** 247
[51] Rossano S, Ramos A, Delaye J-M, Creux S, Filipponi A, Brouder C and Calas G 2000 *Europhys. Lett.* **49** 597
[52] Rossano S, Ramos A Y and Delaye J-M 2000 *J. Non-Cryst. Solids* **273** 48
[53] Ferlat G, San Miguel A, Xu H, Aouizerat A, Blase X, Zuñiga J and Muñoz Sanjosé V 2004 *Phys. Rev.* B **69** 155202
[54] Palmer B J, Pfund D M and Fulton J L 1996 *J. Phys. Chem.* **100** 13393
[55] Wallen S L, Palmer B J, Pfund D M, Fulton J L, Newville M, Ma Y and Stern E A 1997 *J. Phys. Chem.* A **101** 9632
[56] Wallen S L, Palmer B J and Fulton J L 1998 *J. Chem. Phys.* **108** 4039
[57] Fulton J L, Hoffmann M M, Darab J G, Palmer B J and Stern E A 2000 *J. Phys. Chem.* A **104** 11651
[58] Dang L X, Schenter G K and Fulton J L 2003 *J. Phys. Chem.* B **107** 14119
[59] Campbell L, Rehr J J, Schenter G K, McCarthy M I and Dixon D 1999 *J. Synchrotron Radiat.* **6** 310

[60] Spångberg D, Hermansson K, Lindqvist-Reis P, Jalilehvand F, Sandström M and Persson I 2000 *J. Phys. Chem.* B **104** 10467
[61] Jalilehvand F, Spångberg D, Lindqvist-Reis P, Hermansson K, Persson I and Sandström M 2001 *J. Am. Chem. Soc.* **123** 431
[62] Sandström M, Persson I, Jalilehvand F, Lindqvist-Reis P, Spångberg D and Hermansson K 2001 *J. Synchrotron Radiat.* **8** 657
[63] Merkling P J, Muñoz Páez A, Martínez J M, Pappalardo R R and Sánchez Marcos E 2001 *Phys. Rev.* B **64** 012201
[64] Merkling P J, Muñoz Páez A and Sánchez Marcos E 2002 *J. Am. Chem. Soc.* **124** 10911
[65] Park B, Li H and Corrales L R 2002 *J. Non-Cryst. Solids* **297** 220
[66] Okamoto Y 2004 *Nucl. Instrum. Methods Phys. Res.* A **526** 572
[67] Di Cicco A, Filipponi A, Itié J P and Polian A 1996 *Phys. Rev.* B **54** 9086
[68] Raty J Y, Saul A, Gaspard J P and Bichara C 1999 *Phys. Rev.* B **60** 2441
[69] Merkling P J, Ayala R, Martínez J M, Pappalardo R R and Sánchez Marcos E 2003 *J. Chem. Phys.* **119** 6647
[70] Zabinsky S I, Rehr J J, Ankudinov A, Albers R C and Eller M J 1995 *Phys. Rev.* B **52** 2995
[71] Rehr J J and Albers R C 1990 *Phys. Rev.* B **41** 8139
[72] Rehr J J and Albers R C 2000 *Rev. Mod. Phys.* **72** 621
[73] Harfouche M 2003 *PhD Thesis* Université de Marne-la-Vallée
[74] Ankudinov A L, Ravel B, Rehr J J and Conradson S D 1998 *Phys. Rev.* B **68** 7565
[75] Filipponi A, Di Cicco A and Natoli C R 1995 *Phys. Rev.* B **52** 15122
[76] Ottaviano L, Filipponi A, Di Cicco A, Santucci S and Picozzi P 1993 *J. Non-Cryst. Solids* **156–158** 112
[77] Filipponi A, D'Angelo P, Pavel N V and Di Cicco A 1994 *Chem. Phys. Lett.* **225** 150
[78] D'Angelo P, Bottari E, Festa M R, Nolting H F and Pavel N 1997 *J. Chem. Phys.* **104** 2807
[79] Filipponi A 1994 *J. Phys.: Condens. Matter* **6** 8415
[80] Filipponi A and Di Cicco A 2000 *TASK Q.* **4** 575
[81] Crozier E D 1980 *Can. J. Phys.* **58** 1388
[82] Lee P A, Citrin P H, Eisenberger P and Kincaid B M 1981 *Rev. Mod. Phys.* **53** 769
[83] Boyce J, Hayes T and Mikkelsen J J 1981 *Phys. Rev.* B **23** 2876
[84] Hayes T M, Boyce J B and Beeby J 1978 *J. Phys. C: Solid State Phys.* **11** 2931
[85] Filipponi A, Di Cicco A, Tyson T A and Natoli C R 1991 *Solid State Commun.* **78** 265
[86] Gurman S J and McGreevy R L 1990 *J. Phys.: Condens. Matter* **2** 9463
[87] Cormier L, Ghaleb D, Delaye J-M and Calas G 2000 *Phys. Rev.* B **61** 14495
[88] Delaye J-M, Cormier L, Ghaleb D and Calas G 2001 *J. Non-Cryst. Solids* **293–295** 290
[89] Di Cicco A, Minicucci M and Filipponi A 1997 *Phys. Rev. Lett.* **78** 460
[90] Trapananti A and Di Cicco A 2004 *Phys. Rev.* B **70** 014101
[91] March N and Tosi M 1991 *Atomic Dynamics in Liquids* (New York: Dover) ADDRESS
[92] Di Cicco A, Principi E and Filipponi A 2002 *Phys. Rev.* B **65** 212106
[93] Pálinkás G, Bopp P, Jancsó G and Heinzinger K 1984 *Z. Naturf.* a **39** 179
[94] Bichara C, Raty J-Y and Gaspard J-P 1996 *Phys. Rev.* B **53** 206
[95] Raty J Y, Godlevsky V V, Gaspard J P, Bichara C, Bionducci M, Bellissent R, Céolin R, Chelikowsky J R and Ghosez P 2001 *Phys. Rev.* B **64** 235209
[96] Wicks J D, Borjesson L, Bushnell-Wye G, Howells W S and McGreevy R L 1995 *Phys. Rev. Lett.* **74** 726
[97] Wang Y, Lu K and Chenxi L 1997 *Phys. Rev. Lett.* **79** 3664
[98] Winterer M 2000 *J. Appl. Phys.* **88** 5635
[99] Winterer M, Delaplane R and McGreevy R L 2002 *J. Appl. Cryst.* **35** 434
[100] Di Cicco A, Trapananti A and Faggioni S 2003 *Phys. Rev. Lett.* **91** 135505